Investigating the length, area and volume measurement accuracy of UAV-Based oblique photogrammetry models produced with and without ground control points

Erdem Emin Maraş *1 , **Mohammad Noman Nasery** 2

1 Samsun University, Department of Flight Training, Türkiye
2 Ondokuz Mayis University, Department of Geomatics Engineering, Türkiye

Abstract

This study aimed to investigate the performance and sensitivity of 3D photogrammetric models generated without GCPs (ground control points). To determine whether the models with no GCPs retained accuracy in all terrain types as well as under varying climate or meteorological conditions, two separate studies were conducted in two areas with different characteristics (elevation, slope, topography, and meteorological differences). The study areas were initially modelled with GCPs and were later modelled without GCPs. Furthermore, some of the dimensions and areas within the modelled regions were measured using terrestrial techniques (with GPS/GNSS) for accuracy analyses. After regional modelling was conducted with and without GCPs, different territories with different slopes and geometric shapes were selected. Various length, area and volume measurements were carried out over the selected territories using both models (generated with and without GCPs). The datasets obtained from the measurement results were compared, and the measurements obtained using the models produced with GCPs were accepted as the true values. The length measurement results provided various levels of success. The first study area exhibited very promising length measurement results, with a relative error less than 1% and an RMSE (root mean square error) of 0.139 m. In the case of the area measurements, in the first study area (Sivas), a minimum relative error of 0.04% and a maximum relative error of 1.05% with an RMSE of 1.264 m² were obtained. In the second study areas (Artvin), a minimum relative error of 0.56% and a maximum relative error of 5.27% with an RMSE of 1.76 m² were achieved. Finally, in the case of the volume measurements, for the first study area (Sivas), a minimum relative error of 0.8% and a maximum relative error of 6.8% as well as an RMSE of 2.301 m³ were calculated. For the second study area (Artvin), the minimum relative error of the volume measurements was 0.502%, and the maximum relative error was 2.01%, with an RMSE of 7.061 m³.

1. Introduction

Photogrammetry, especially digital photogrammetry, is a versatile tool used for aerial surveys and is rapidly becoming the tool of choice for generating 3D realistic models from 2D photos for different engineering projects. Three-dimensional modelling via digital photogrammetry is based on a combination of vertical and inclined imagery. Oblique photogrammetry offers improved capabilities for the 3D reconstruction of different surfaces and terrains. Three-dimensional models obtained via oblique photogrammetry have widespread uses in different engineering fields, and their

application area is expanding daily due to recent advances in technology, hardware, and software development. Currently, digital photogrammetry has numerous potential applications in areas such as surveying, civil engineering, urban planning, architecture, archaeology, mining, mass movement monitoring, industry, urban management, agriculture, and real estate.

Digital photogrammetry or three-dimensional (3D) mapping, the most famous discipline of the digital age, is expanding quickly and intensely around the world due to the low-cost facilities required for data acquisition and rapid workflow. Basically, UAV photogrammetry makes

the three-dimensionally (3D) reconstruction of objects via two-dimension (2D) photos possible. In addition, a model produced via oblique photogrammetry does not aim to just view and display the output object but also provides accurate geometric and spatial information about the object. In oblique photogrammetry, UAVs (unmanned aerial vehicles), also known as drones, are used to obtain aerial imagery. Recently, UAV photogrammetry has been used in different areas such as cultural heritage documentation [1-2], agriculture [3-4], architectural restoration [5-6], archaeology [7-8], mining [9-10], coastal habitat monitoring [11], and urban and infrastructure planning [12]. Older, challenging data acquisition methods have been eliminated by photogrammetry. Since 2D cadastre information does not meet today's needs, the world is moving into the 3D cadastre system, the name of which clearly shows that 3D information is needed for its applications and that such information could be supplied just with oblique photogrammetry [13-14]. Three-dimensional photogrammetric modelling plays an important role in designing three-dimensional city models as well as in urban management applications, especially during the city planning stage, it helps urban planners make optimal city plans.

Yılmaz [15] stated that the insufficiency of two-dimensional cadastre information for solving the problems occurring due to the lack of three-dimension information reveals the need for 3D cadastre implementation. Mueed Choudhury [16] used UAV-based oblique photogrammetry for the purpose of determining the characteristics of city trees, modelling a specific area for this purpose and determining the characteristics of city trees through this three-dimensional model. Wu et al. [17] used a new method in which aerial images were combined with terrestrial images, and they obtained good 3D city models with proper building geometries to obtain better 3D city models. One study called "Quantifying uncertainties in snow depth mapping from structure from motion photogrammetry in an alpine area" used the structures obtained from motion photogrammetry to characterise spatial uncertainties in snow depths [18]. For this purpose, a study was conducted at the Combe de Laurichard, which is located in the French Alps. Two different dates, June 1st, 2017 and October 5th, 2017, were chosen (one snow-on and one snow-off condition) for aerial data acquisition, and two DEMs (digital elevation models) from two datasets were constructed and compared; in this study, a method was presented for calculating spatially varying estimates of the snow depth precision and detection limits using repeated UAV surveys. Chudley et al. [19] called "High-accuracy UAV photogrammetry of ice sheet dynamics with no ground control points", the application of an alternative SFM-MVS (structure from motion-multi-view stereo) geolocation method called GNSS-supported aerial triangulation was presented; in this method, a carrier-phase GNSS receiver located onboard geo-references the SFM-MVS point cloud, significantly reducing the need for GCPs. Considering various flight configurations such as linear strips, radial strips and curved strips, the diverse obtained datasets were evaluated in terms of the density of the extracted point clouds and the distance between the reconstructed surface and control points [20].

Tomaštik et al. [21] conducted a study using a flight in the study area in which there was a 300-metre height difference; the vegetation cover in this region was forests. In this study, RMSE values were obtained as a result of comparing products such as orthophotos and digital surface models (DSMs) produced GCPs and without using GCPs, with these control points determined in the field. The RMSE values obtained by using GCP were between 8 cm and 20 cm horizontally and between 16 cm and 62 cm vertically. When the RMSE values obtained without using GCP were examined, the authors determined that, while the values varied between 6 cm and 9 cm horizontally, they varied between 8 cm and 15 cm vertically.

He et al. [22] obtained RMSE values of 1-3 cm horizontally and 4 cm vertically in a study area with different terrain types. Gerke and Przybilla [23] obtained horizontal and vertical RMSE values below 10 cm without using GCPs on a land surface with a maximum height difference of 50 metres. At the same time, they obtained similar results by using GCPs.

Türk and Öcalan [24], after establishing and marking 9 GCPs in the campus of Sivas Cumhuriyet University, a photogrammetric flight was performed by UAV equipped with PPK. Images obtained from this flight were processed by Pix4D, a photogrametric processing software, following different strategies as: with GCPs and without GCPs. The accuracy of the ortho-image produced using GCPs was obtained as 3.6 cm in horizontal and 5.0 cm in vertical.

2. Definition of problem

As a matter of fact, GCPs are a mandatory factor used to generate an accurate photogrammetric model, but what if GCPs cannot be marked due to location inaccessibility issues, such as lands with high slopes (canyons) or vertical structures (dam bodies), insufficient project budgets, areas with landslide risks or some other hazardous field situations such as glaciated environments? Modelling such land terrains and structures with GCPs is sometimes impossible or requires a vast budget. Should a photogrammetric model without GCPs be deemed as accurate as a model utilizing GCPs for some engineering applications?

3. The aim of this study

The purpose of this paper is to indicate the usability of photogrammetric models generated without GCPs in some engineering application such as length, area, and volume measurements.

For this purpose, two different areas with different characteristics were modelled with and without GCPs. The areas and lengths of these areas were measured using orthophotos, and the volumes were calculated from DEMs.

The measurements mentioned above were conducted over the same areas in both models produced with and without GCPs, and the results are discussed in detail.

4. Methods

A DJI Phantom 4 Pro Drone with a GPS/GLONASS satellite positioning system, a vertical hover accuracy of ±0.1 m and a horizontal hover accuracy of ±1.5 m and a 20 MP (Mega Pixel) camera were used for data acquisition in this study. In contrast, the use of real-time kinematic or post-processing kinematic enabled GNSS devices allows to improve the spatial accuracy to a range of several centimeters [25]. DJI Terra's Oblique Mission uses 5 flight routes to capture the same amount of data as that obtained using 5 cameras simultaneously on a drone. The 5 flight routes correspond to the 5 camera headings – downward, forward, backward, leftward, and rightward.

To measure the GCPs, a GEOMAX Zenith40-type GPS/COARS with 72 channels (GPS/GLONASS) was used in conjunction with a Maximum 36 satellite signal receiver; the satellite signal tracking capacity of GPS is L1, L2, L2C, and that in GLONASS is L1, L2.

The GNSS raw data were post-processed by RTKLib open-source software in the carrier-phase differential mode with respect to the CHC X91 model GNSS receiver mentioned in Section 5.1 as base station. The ratio of epochs with a fixed solution to total epochs of the GNSS trajectory solution is 99.17% and the mean standard deviation along x, y and z axes amounts to 8.4, 5.5 and 9.6 mm, respectively.

DJI RTK systems offer, due to the availability of the original satellite observation data as well as ephemeris data, the possibility of an improved position determination in post-processing. The necessary calculations can be performed using the free software RTKLIB [26]. RTKLIB is an open-source program package for standard and precise positioning with GNSS. RTKLIB consists of a portable program library and several APs (application programs) utilizing the library.

5. Case study

To investigate the usability of 3D (three-dimensional) photogrammetric models generated without GCPs, two studies were conducted in two different provinces of Turkey with different characteristics. The first area, Sivas, is located in southern Turkey with an elevation of 1650 m (above sea level), and the second area, Artvin, is located in north-eastern Turkey with an elevation of 450 m. The large elevation difference between these two regions as well as other varying factors such as meteorological differences, slope differences, terrain topography differences, etc., are applied to investigate whether the studied principle is applicable everywhere. The two areas were modelled one time with GCPs and another time without GCPs. The data acquisition process in both areas was as follows.

5.1. Sivas

This study region is presented in Fig. 1; research was conducted in Şuğul Canyon, located in the Sivas province of Turkey. Oblique imagery of this study area was obtained, and with the help of these data, the area was modelled with and without GCPs to compare the sensitivities of the two models in measuring the lengths, areas and volumes of the same regions.
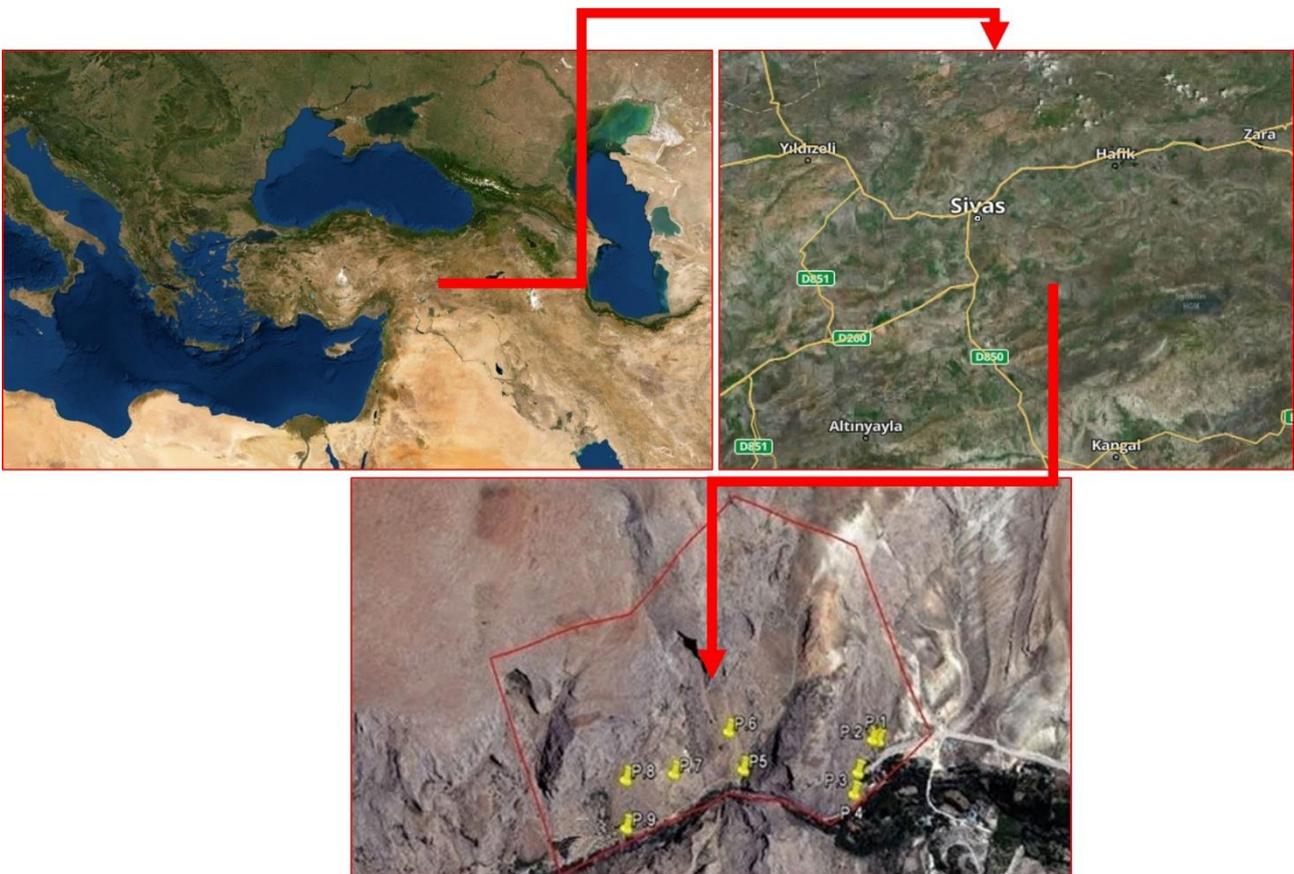

Figure 1. First study area Sivas, Gürün, Şuğul Canyon, Turkey

Figure 2. DJI Phantom 4Pro model UAV and CHC X91 model RTK-GNSS receiver used for data acquisition

Figure 3. Marking and measuring GCPs

To model the area with the oblique aerial photogrammetry method, a DJI Phantom 4 Pro model UAV was used (Fig. 2). Nine well-distributed GCPs were used to geo-reference the model. The GCP measurements were conducted with an RTK-GNSS receiver (CHC X91 GNSS model).

First, 9 well-distributed ground control points were established in the study area; during the establishment of these points, care was taken to ensure that they could easily be seen in the photos and were located away from any natural or artificial objects such as trees and buildings that would prevent these points from appearing in the pictures (Fig. 3).

After establishing the GCPs, the locations of these points were recorded in the Turkish National Reference System as TUREF/TM36 (ITRF96 in the universal system as EPSG: 5256) with a sensitivity of 2 cm; the obtained coordinates are given in Table 1.

Next, the flight plan and flight time were determined. Because the study area was mountainous, the appropriate flight time was determined as 12:00–14:00. Selecting this time frame allowed the effect of shading that would cause errors in the photogrammetric evaluation to be minimized. A DJI Phantom 4 Pro model UAV was used for the aerial photography; this Phantom 4 Pro was equipped with a 20-MP camera that could take photos with 4K quality and had a 1-inch sensor. The DJI Phantom 4 Pro model UAV camera is presented in Fig. 4.

Table 1. Coordinate list of ground control points

| Point No.	X (m) East	Y (m) North	Z (m) Ellipsoidal Height
P.1	607223.539	4292394.086	1401.258
P.2	607217.702	4292407.654	1409.344
P.3	607141.923	4292390.866	1394.211
P.4	607094.008	4292376.559	1391.703
P.5	606994.953	4292671.055	1446.086
P.6	606986.964	4292597.873	1407.067
P.7	606845.780	4292703.114	1445.776
P.8	606793.686	4292683.833	1415.525
P.9	606664.304	4292784.330	1447.985

Figure 4. Phantom 4Pro UAV camera
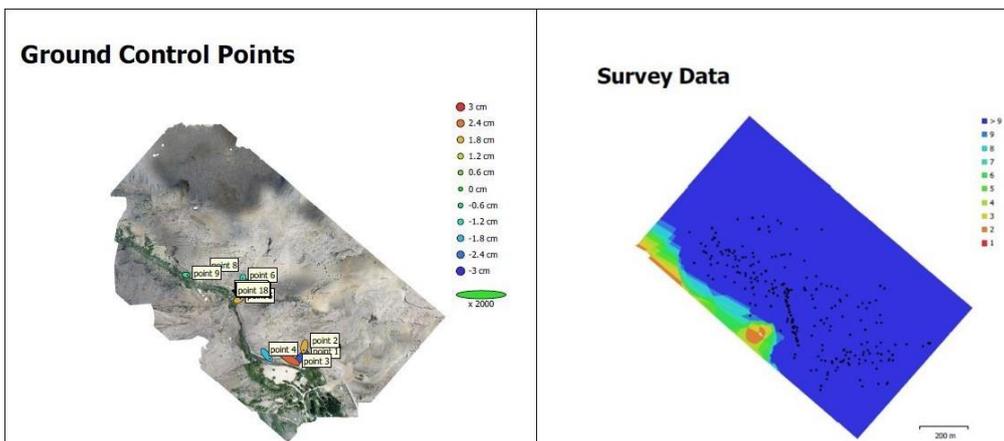
Figure 5. GCP positions and image overlap

The images were taken with the above-described UAV, and nadir and oblique images of the study area were obtained. The overlap in the imagery was 85%, and the forward overlap was 80%; these overlap percentages are sufficient to represent the topography and to virtually reconstruct the study area in three dimensions. The GCP positions and image overlap ratios are given graphically in Fig. 5.

The internal orientation parameters and camera calibration values used in the photogrammetric evaluation phase are presented in Table 2. The F values listed in this table indicate the focal length of the camera, Cx-Cy coordinates of the prime point, B1-B2 non-orthogonal transformation coefficients, K1-K2-K3 radial distortion values, and P1-P2 tangential distortion values. The GCP errors calculated by the Agisoft/Metashape and are given in Table 3.

Afterwards, the obtained aerial photographs were subjected to a photogrammetric evaluation, and the measured GCP coordinates were also used during this evaluation. Finally, the geometry of the subject area was reconstructed formally and computationally in virtual form. As a result of the evaluation, a dense cloud including 8,193,681 points with global coordinates, a 3D model, and an orthophoto and digital elevation model were obtained, as shown in Fig. 6.

Interpolation is a mathematics and statistical approach to estimation problems. In addition, in digital terrain modelling, interpolation is used to determine the elevation value of a given point benefiting from the known elevations of neighbouring points. There are two implicit assumptions behind interpolation techniques:

• The land surface is continuous and smooth.
• There is high correlation among neighbouring data points.

Interpolation is a basic technique in digital terrain modelling because it can be applied within various phases of the modelling process, such as in surface reconstructions, quality control, accuracy assessments, land analyses and implementations. In this study, a digital terrain model was produced by linear interpolation.

After a 3D model was generated with GCPs, a 3D model of the work area was again generated, this time without GCPs. The three-dimensional models created with and without GCPs are not presented separately as they are not visually different from each other.

5.2. Artvin

The second study site was the Artvin dam built on the Çoruh River, which is located in the Artvin province of Turkey (Fig. 7). Three-dimensional models of the area were generated by oblique photogrammetry, once with and once without GCPs.

To model this study area via aerial photogrammetry methods, a DJI Phantom 4 Pro model UAV was used. Five GCPs were used to geo-reference the model. The GCP measurements were conducted with a TRIMBLE R6 GPS (CORS/GNSS) receiver (Fig. 8). The coordinates of the GCPs were recorded in the Turkish National Reference System as TUREF/TM42 (3-degree) (ITRF96 in the universal system as EPSG: 5258) with a sensitivity of 2 cm, and the obtained coordinates are given in Table 4.

Table 2. Correlation matrix calculated by the Agisoft/Metahshape software

	Value	Error	F	Cx	Cy	B1	B2	K1	K2	K3	P1	P2
F	**3656.51**	0.04	1.00	0.00	0.20	-0.28	0.04	-0.21	0.25	0.23	0.00	-0.19
Cx	**-4.57**	0.08		1.00	0.01	-0.02	0.04	0.01	0.00	0.00	0.94	-0.01
Cy	**18.41**	0.06			1.00	-0.21	0.00	-0.03	0.02	-0.02	0.00	0.85
B1	**-7.25**	0.02				1.00	0.02	-0.02	0.00	0.00	-0.01	0.06
B2	**0.36**	0.02					1.00	0.00	0.00	0.00	-0.12	0.01
K1	**0.01**	0.01						1.00	-0.97	0.91	0.00	-0.04
K2	**-0.01**	0.01							1.00	-0.97	0.91	0.02
K3	**0.02**	0.01								1.00	0.00	-0.02
P1	**-0.01**	0.01									1.00	-0.01
P2	**-0.01**	0.01										1.00

Table 3. GCP errors calculated by the Agisoft/Metashape software

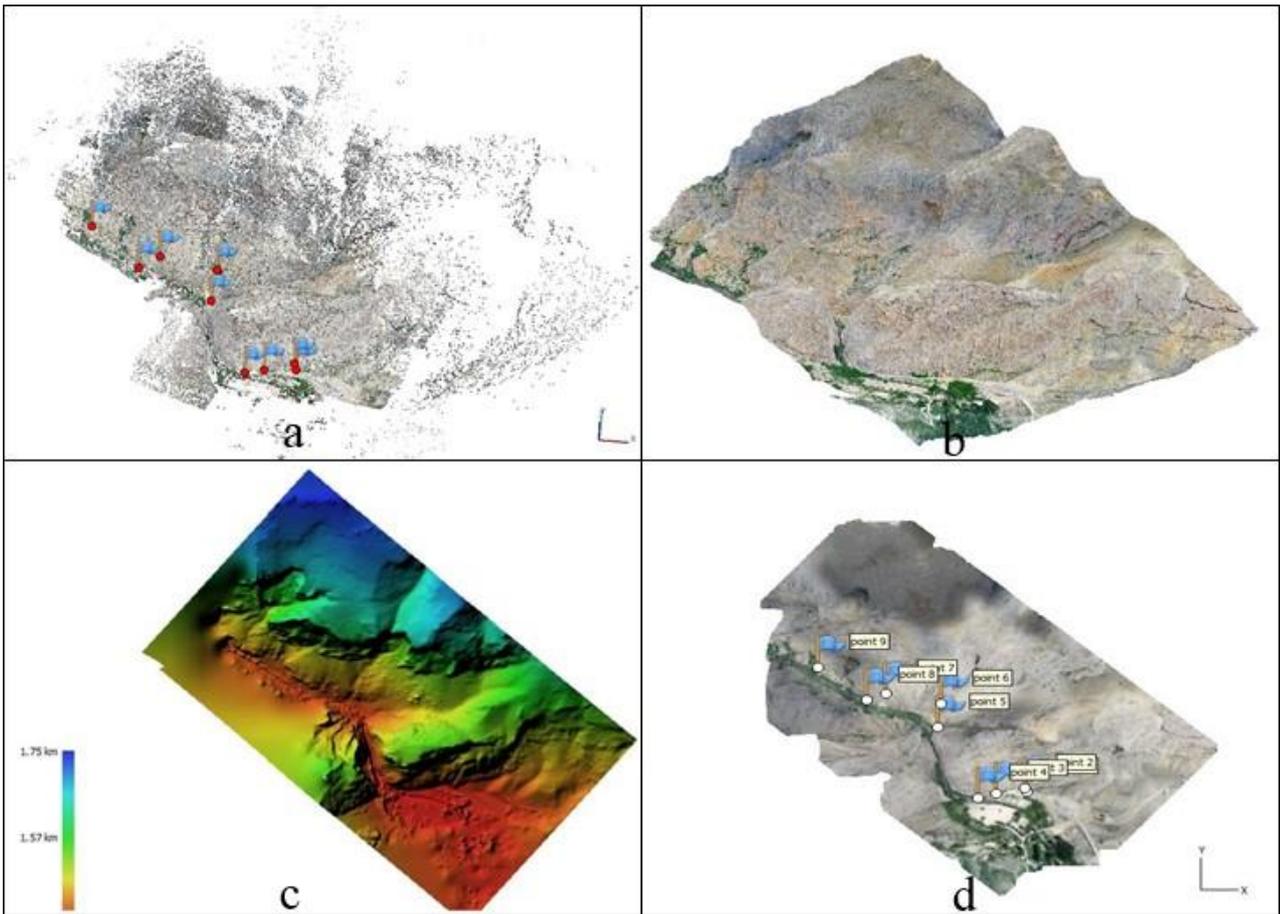| Label	X error (cm)	Y error (cm)	Z error (cm)	Total (cm)	Image (pix)
P.1	1.273	1.163	-2.676	3.184	0.320 (17)
P.2	-0.265	-1.345	1.950	2.384	0.299 (21)
P.3	-2.428	1.455	2.572	3.825	0.333 (15)
P.4	1.162	-1.346	-1.782	2.518	0.198 (22)
P.5	0.637	0.363	1.899	2.036	0.117 (5)
P.6	-0.113	-0.228	-1.186	1.213	0.201 (17)
P.7	-0.694	-0.402	0.301	0.858	0.087 (5)
P.8	0.479	-0.046	-0.851	0.977	0.067 (6)
P.9	0.017	0.190	0.491	0.527	0.063 (7)
Total	**1.058**	**0.912**	**1.727**	**2.221**	**0.246**

Figure 6. Results of photogrammetric evaluation a) Tie Points b) 3D model c) Digital Elevation Model d) Orthophoto
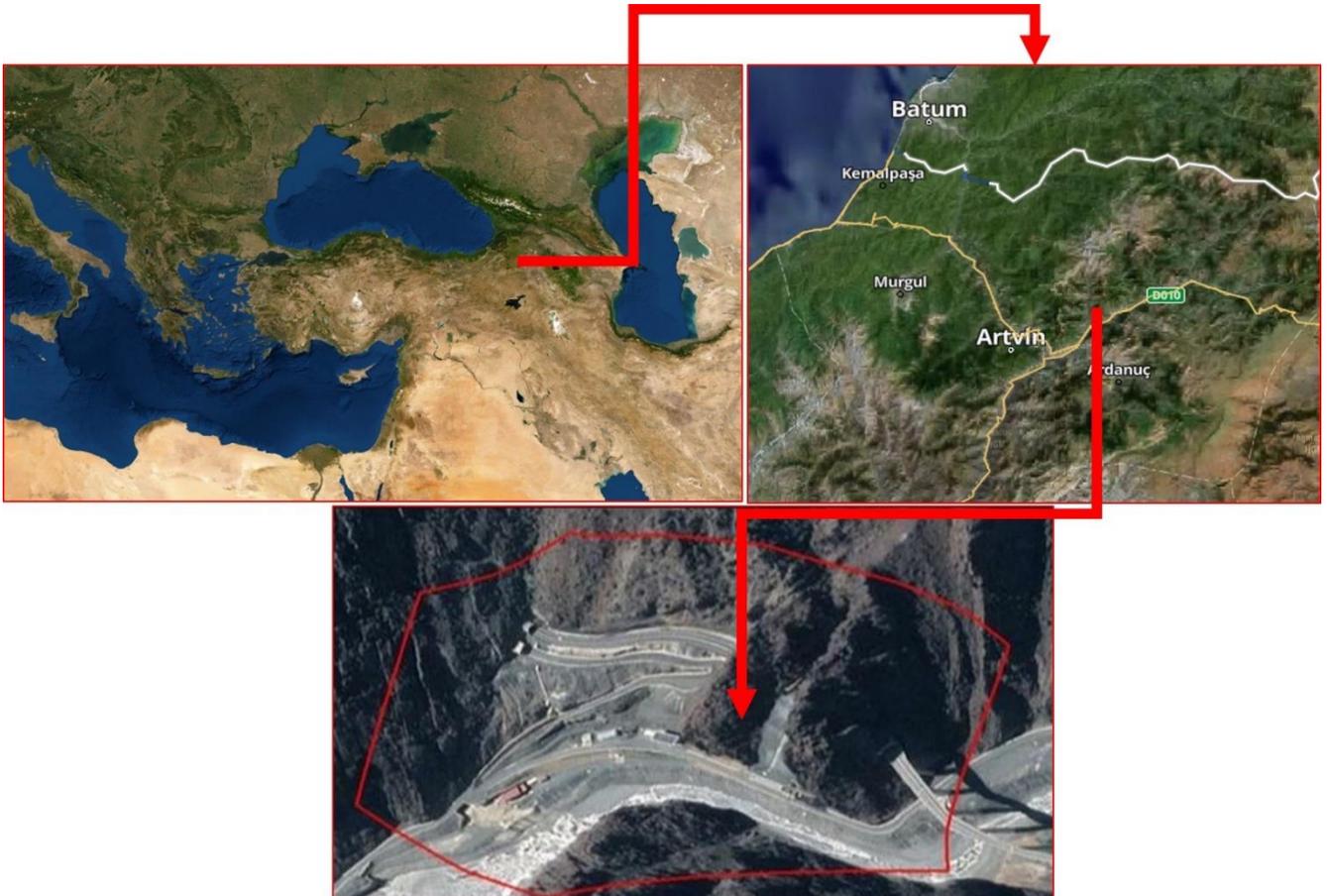

Figure 7. Second Study area Turkey, Artvin, Artvin Dam

Table 4. GCP coordinate list

Point No.	X (m) East	Y (m) North	Z (m) Ellipsoidal Height
P1	480173.041	4534136.386	408.183
P2	480193.098	4534080.037	395.799
P3	480188.260	4533962.940	397.686
P4	480112.801	4534002.926	442.610
P5	480095.596	4533966.277	446.039

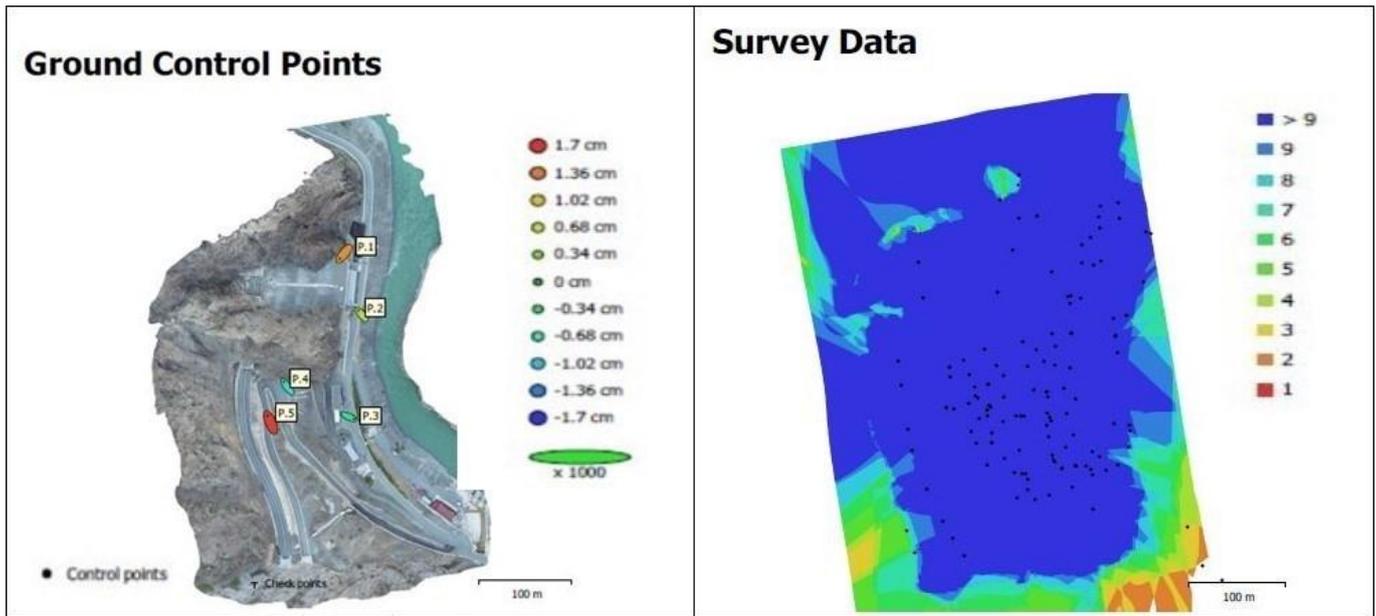**Figure 8.** Equipment used to obtain datasets

Figure 9. GCPs positions and image overlaps Orthophoto

The imagery was derived using the UAV in accordance with photogrammetric principles, and as a result, nadir and oblique images were obtained. The overlap in the imagery was 85%, and the forward overlap was 80%; these overlap percentages are sufficient to represent the topography and to virtually reconstruct the study area in three dimensions. The GCP positions and image overlap ratios are given in Fig. 9.

The positions and errors of the GCPs used during the photogrammetric evaluation, the image overlap ratios, the camera calibration coefficients and the correlation matrix are shown graphically in Fig. 9. The correlation matrix is given in Table 5. The GCP position errors were also calculated and are listed in Table 6.

Afterwards, the obtained aerial photographs were processed in accordance with photogrammetric principles, and the measured GCP coordinates were also used during the photogrammetric processing of the images. Finally, geometry of the subject area has been reconstructed formally and computationally in virtual form. As a result of this process, a dense cloud including 18,958,130 points with global coordinates, a 3D model, an orthophoto and a digital elevation model were obtained, as shown in Fig. 10.

After reconstructing the study area virtually in three dimensions using GCPs, a 3D model was generated without GCPs. The 3D models created with and without GCPs are not presented separately as they are not visually different from each other.

Table 5. Correlation matrix calculated by the Agisoft/Metashape software

	Value	Error	F	Cx	Cy	B1	B2	K1	K2	K3	P1	P2
F	3649.93	0.05	1.00	0.01	0.35	-0.09	0.05	-0.33	0.34	-0.31	-0.07	0.06
Cx	-3.28	0.06		1.00	0.12	0.03	0.04	0.01	-0.02	0.02	0.69	-0.23
Cy	16.63	0.06			1.00	-0.06	0.06	-0.03	0.01	0.00	0.32	-0.31
B1	-0.28	0.02				1.00	0.01	0.01	-0.02	0.02	0.01	-0.01
B2	0.21	0.02					1.00	0.00	0.00	0.00	-0.10	0.03
K1	0.01	0.01						1.00	-0.97	0.93	0.01	-0.01
K2	-0.04	0.01							1.00	-0.99	-0.02	0.01
K3	0.07	0.01								1.00	0.02	-0.01
P1	-0.01	0.01									1.00	0.79
P2	-0.01	0.01										1.00

Table 6. GCP position errors given by the Agisoft/Metashape software

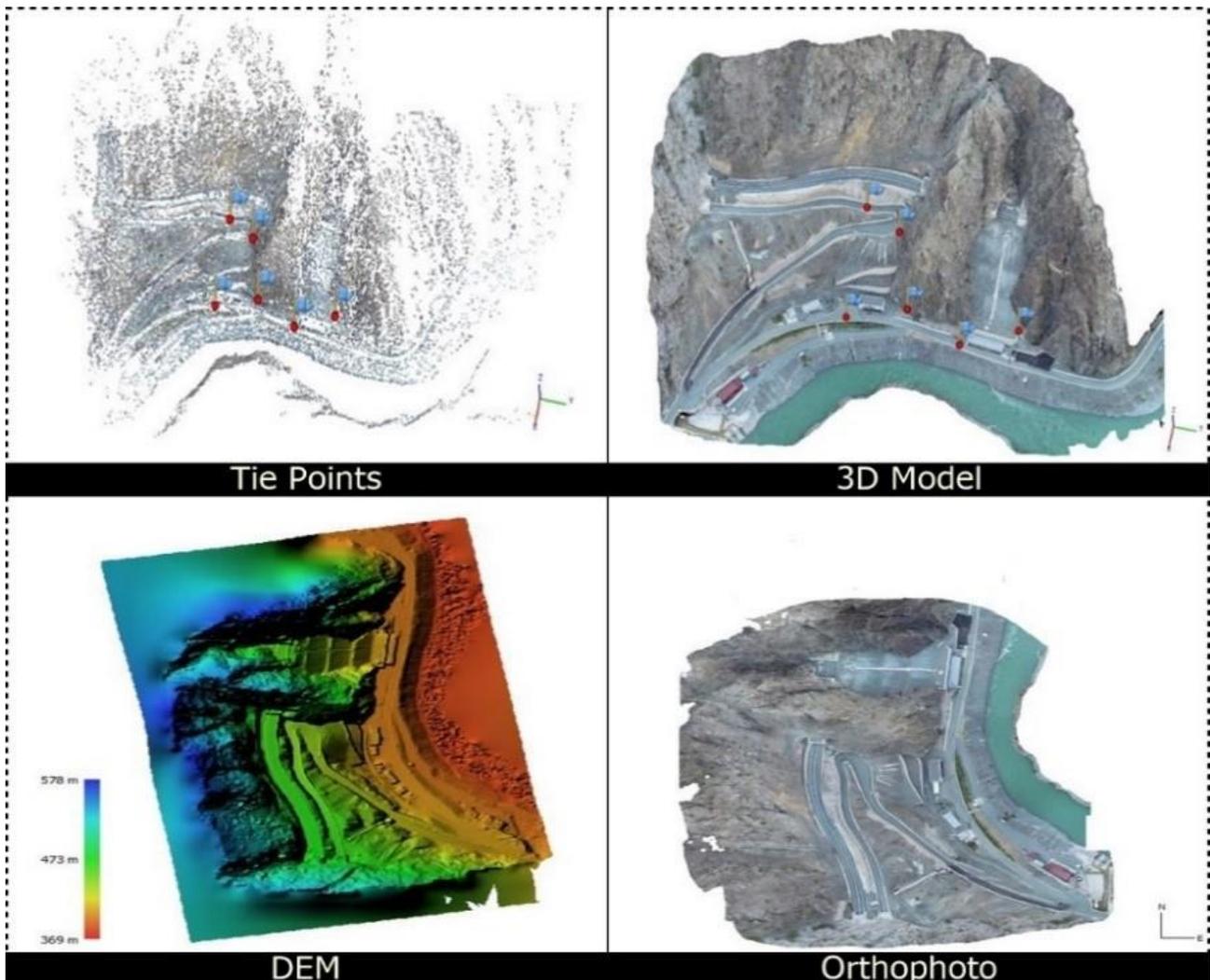| Label	X error (cm)	Y error (cm)	Z error (cm)	Total (cm)	Image (pix)
P.l	-0.93064	-1.11915	1.23013	1.90573	0.321 (18)
P.2	-0.68080	0.83722	0.64880	1.25912	0.206 (21)
P.3	1.10243	-0.46048	-0.47225	1.28468	0.425 (14)
P.4	-0.78656	1.07360	-0.71107	1.50895	0.543 (8)
P.5	-0.61781	1.47969	1.62688	2.28427	0.245 (32)
Total	**0.84206**	**1.04953**	**1.03049**	**1.69484**	**0.320**

Figure 10. Tie Points, 3D Model, Digital Elevation Model and Orthophoto

6. Findings and Examination

In this section, an accuracy assessment is initially conducted for the models generated with GCPs. Afterwards, a comparison study is done among the final 3D models (one with GCPs and other without GCPs) obtained from the photogrammetric process. The length, area and volume measurements are selected as the comparison criteria. These measurements were collected in different areas using the models generated with and without GCPs, and at the end, these results were compared to the corresponding measurement conducted with terrestrial methods (GPS/GNSS), and the results are compared in detail.

6.1. Assessment of the length, area and volume measurements

6.1.1. First study area (Sivas) experimental studies

Length, area, and volume measurements of areas with different geometric shapes and slopes are carried out for the first study area.

6.1.2. Length measurement for accuracy analyse of model

Initially, two areas are selected for the accuracy analyses of the two models, length measurements are obtained for the study areas using the terrestrial method (using RTK (Real Time Kinematic/GNSS)), and the same areas are finally measured using the two models (the model with GCPs and the model without GCPs). The results of the measurements are given in Table 7.

As seen in Table 4, our model is sufficiently sensitive. Because the measurements are close enough to the data obtained with RTK/GNSS, the model generated with GCPs is sufficiently accurate, and since we could not measure all investigated areas with the terrestrial method in this study, the data obtained from the model with GCPs are accepted as true values, while the other data (obtained from the model without GCPs) are compared to these data. Different features are measured with both models, as shown in Fig. 11.

After the model accuracy is confirmed, measurements are conducted using both models in areas with different shapes. The measurements are provided in Table 8 and are further compared. The measurements obtained with the two models are graphically shown in Fig. 12.

Table 7. Length measurements obtained with different methods

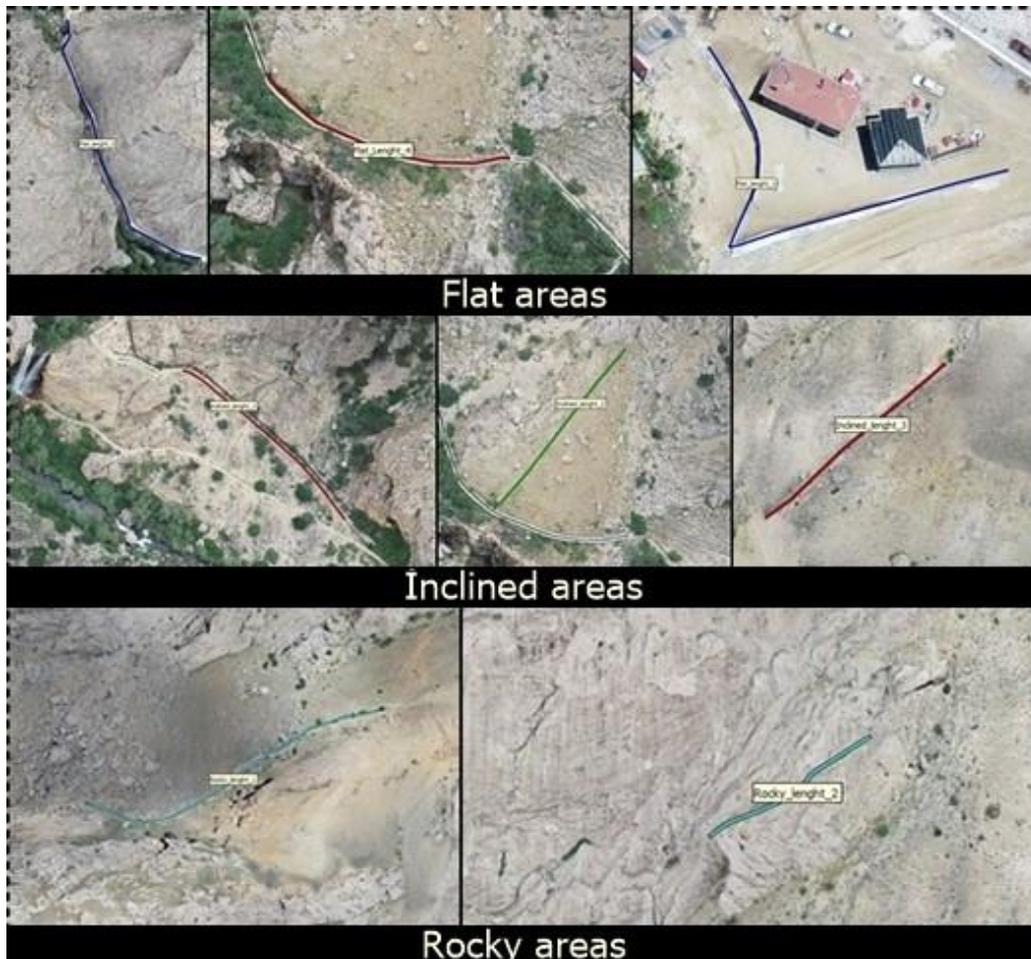| Area Name	Reference (With GPS) (m)	With GCPs (m)	Without GCPs (m)	*RMSE (mm)*	Relative Error %
1	13.830	13.817	13.804	0.020	0.14
2	14.770	14.765	14.792	0.016	0.11

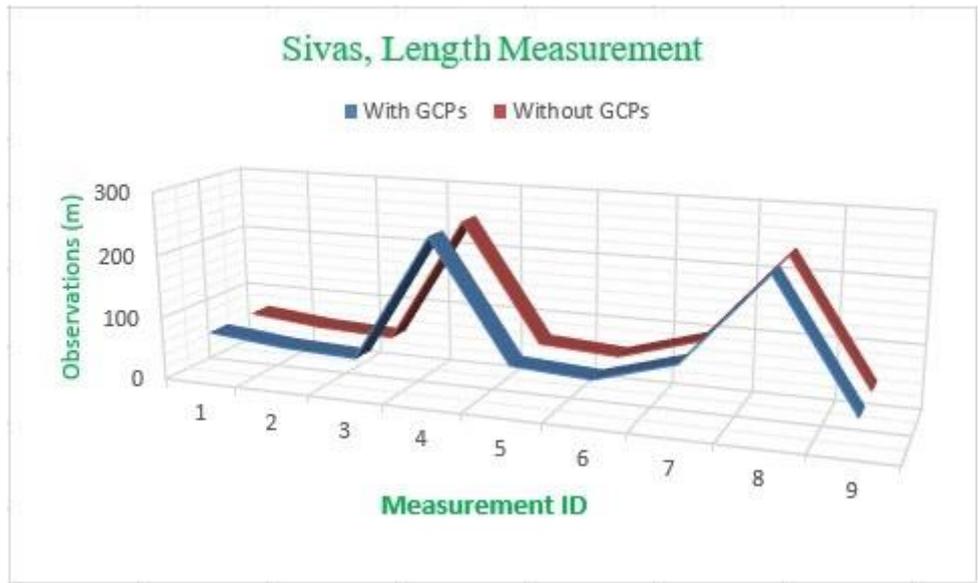**Figure 11.** Length measurements of areas with different topography

Figure 12. Measurements done in two models are graphically indicated

6.1.3. *Length measurement for accuracy analyze of model*

To observe the usability of the model produced without GCPs for the application of area measurements, 5 areas with different features are measured using both models, as shown in Fig. 13. The area measurement results are given in Table 9. The measurements conducted using the two models are shown graphically in Fig. 14.

Table 8. Length measurements obtained from two models of Sivas for the same areas

Area Type	With GCPs (m)	Without GCPs (m)	Δi (m)	Relative Error %	RMSE (m)
	72,418	72,470	-0,052	0,100	
Flat Areas	60,518	60,558	-0,040	0,100	
	55,466	55,424	0,042	0,100	
	253,182	253,083	0,099	0,040	
Inclined Areas	69,644	69,746	-0,102	0,150	**0,139**
	61,672	61,541	0,131	0,210	
	98,036	98,230	-0,194	0,200	
Rocky Areas	238,598	238,346	0,252	0,110	
	47,944	47,821	0,173	0,360	
		Mean	**0,121**	**0,126**	

Table 9. Area measurements carried out with both models for the same areas

First Study Area (Sivas) Measurements					
Observation No.	With GCPs (m²)	Without GCPs (m²)	Δi (m²)	Relative Error %	RMSE (m²)
Flat Areas	2789.200	2788.100	1.100	0.040	
	682.526	683.594	-1.068	0.160	
	1277.400	1278.700	-1.300	0.100	**1.264**
Inclined Areas	854.864	853.288	1.576	0.180	
	115.021	113.810	1.211	1.050	
		Mean	**1.251**	**0.306**	

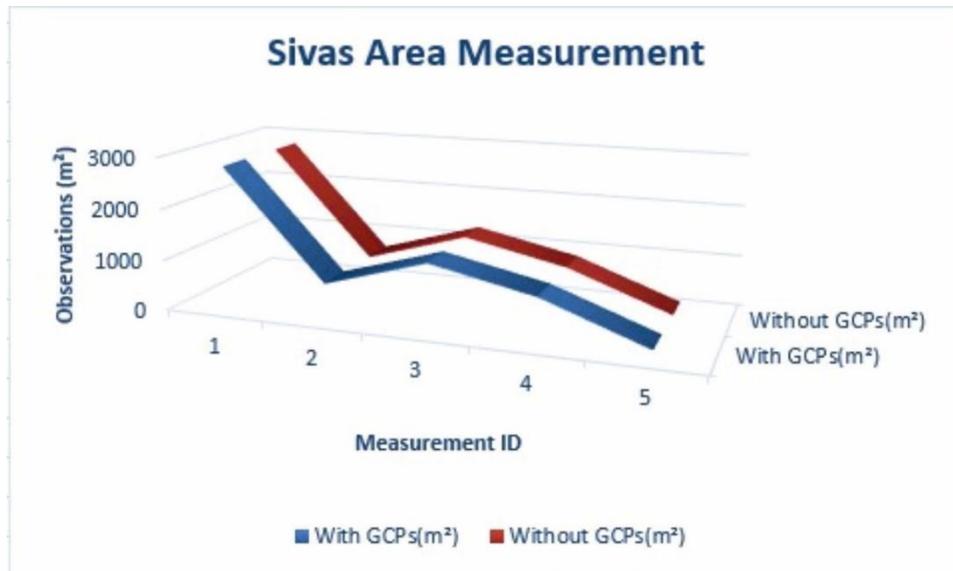**Figure 13.** Area measurements done over both models

Figure 14. Measurements done in two models are showed graphically

6.1.4. Volume Measurements for Sivas

In order investigate the usability of the model generated without GCPs regarding volume measurements, the volumes of 4 different rocks were measured using both models, as shown in Fig. 15.

In Photoscan, the "reference surface" to be used for volume calculations can only be a plane. This surface can be defined in three ways:

• as an inclined flat surface interpolated by the vertices of the delimitation of the object (best-fit plane).
• as a horizontal flat surface with a moderate height determined by the heights of the vertices of the delimitation of the object (mean-level plane);
• as a horizontal flat surface at a reference height determined by the user (custom-level plane).

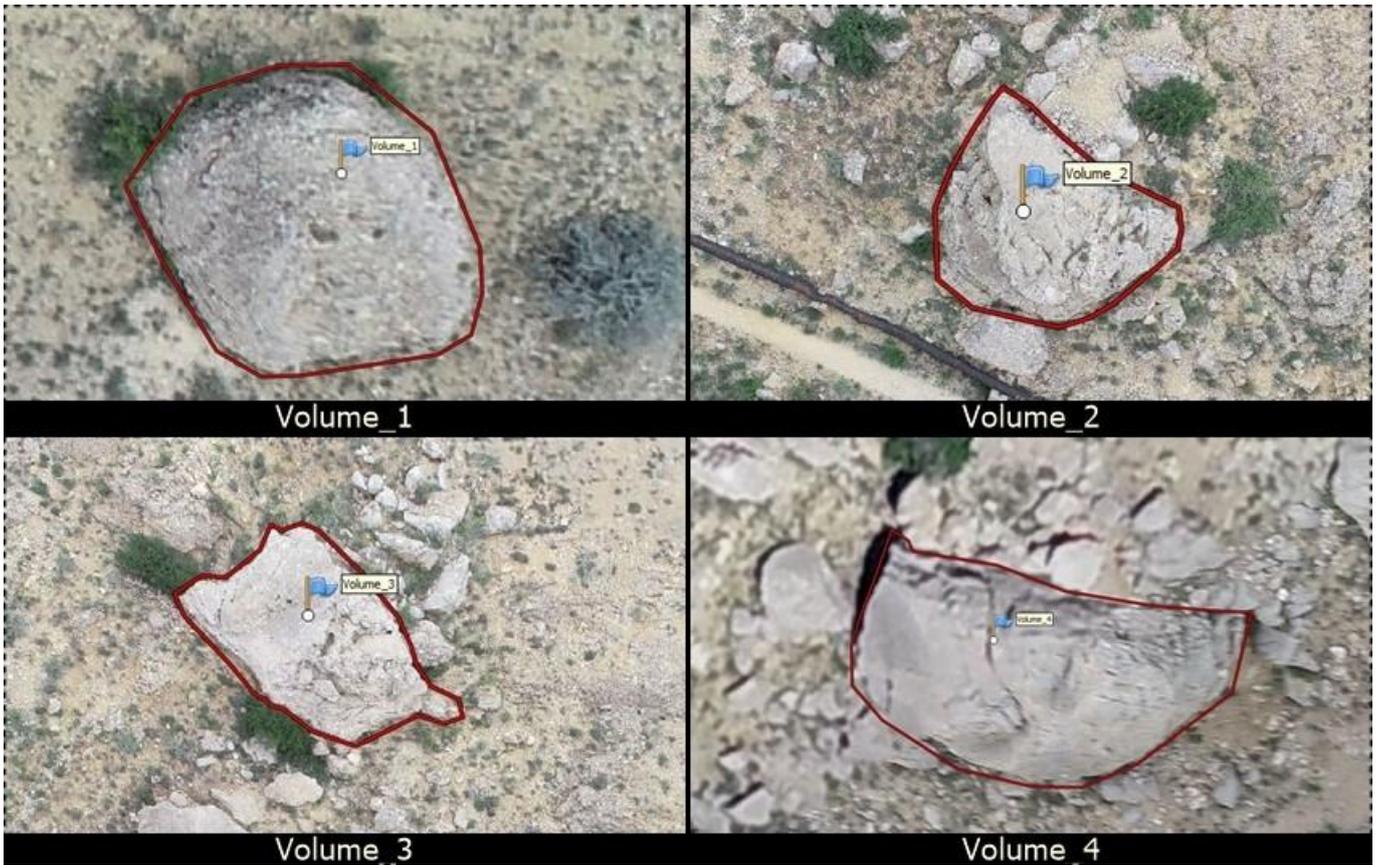The results of the volume measurements are provided in Table 10 and Fig. 16.

43

Figure 15. Volume measurements of 4 rock done within both models

Table 10. Volume measurements and RMSEs

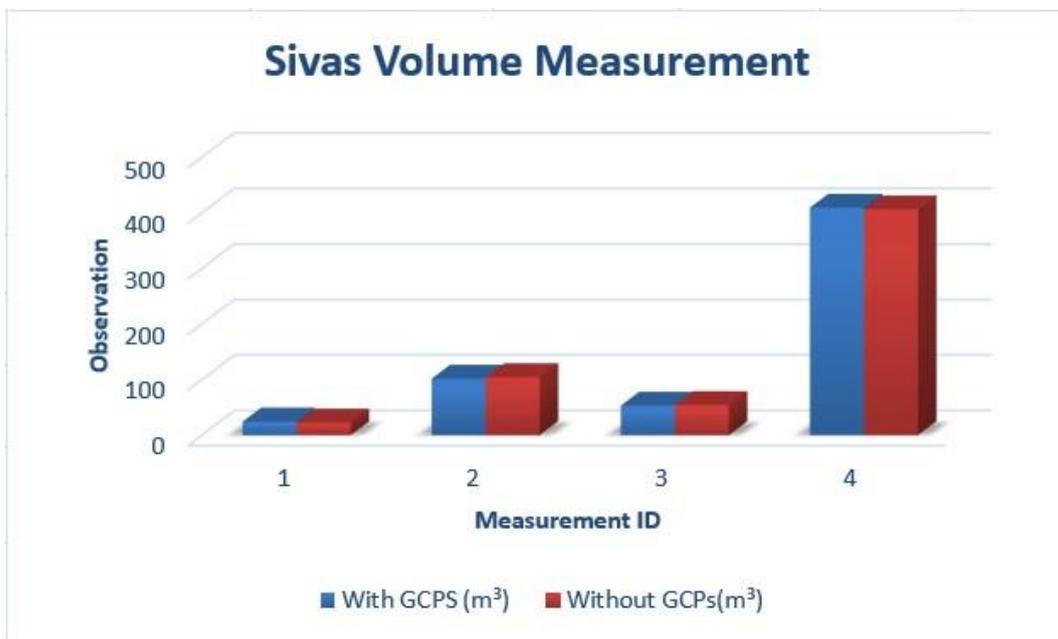| First Study Area (Sivas) Volume Measurements					
Observation No.	**With GCPS (m³)**	**Without GCPs (m³)**	**Δi (m³)**	**Relative Error %**	**RMSE (m³)**
1	24.119	22.478	1.641	6.800	
2	101.393	104.088	-2.695	2.660	
3	52.881	54.043	-1.162	2.200	**2.301**
4	409.243	406.101	3.142	0.80	
		Mean	**2.160**	**3.115**	

Figure 16. Volume measurements are shown graphically

6.2. Artvin Area's experimental studies (Second study area)

As in the last section, the length, area and volume measurements are conducted using the two models, and the results of the measurements obtained with both models (with and without GCPs) are given in Table 11.

6.2.1. Length measurements

The lengths of regions with different shapes were measured, as shown in Fig. 17, and the measurements are given in Table 12. A graphical interpretation of the length measurements is shown in Fig. 18.

6.2.2. Area measurements of the second study area (Artvin)

The areas of different objects are measured using both models, and the results are given in Fig. 19. A graphically representation of the area measurements is given in Fig. 20.

6.2.3. Volume measurements of second study area (Artvin)

The volumes of different objects are measured for the intended goal of investigating the usability of the model generated without GCPs, and the results are shown in Fig. 21.

6.2.4. Volume measurements of second study area (Artvin)

The volumes of different objects are measured for the intended goal of investigating the usability of the model generated without GCPs, and the results are shown in Fig. 21.

The measured volume values are given in Table 13. The volumes measured using both models are shown graphically in Fig. 22.

Table 11. Measured length values

Second Study Area (Artvin) Length Measurements					
Observation No.	With GCPs (m)	Without GCPs (m)	Δi (m)	Relative Error %	RMSE (m)
1	209.522	209.303	0.219	0.100	
2	69.293	69.199	0.094	0.140	0.153
3	58.667	58.552	0.115	0.200	
		Mean	0.143	0.147	

Table 12. Area measurements from both models

Second Study Area (Artvin) Area Measurements					
Observation No.	With GCPs (m^2)	Without GCPs (m^2)	Δi (m^2)	Relative Error %	RMSE (m^2)
1	215.045	212.828	1.207	0.560	
2	27.967	26.494	1.473	5.270	1.726
3	65.567	63.263	2.304	3.510	
		Mean	1.661	3.113	

Table 13. Volume measurements and RMSEs

Second Study Area (Artvin) Volume Measurement					
Observation No.	With GCPS (m^3)	Without GCPs (m^3)	Δi (m^3)	Relative Error %	RMSE (m^3)
1	2129.885	2118.759	11.126	0.520	
2	161.364	158.123	3.241	2.010	7.061
3	779.396	775.485	3.911	0.502	
		Mean	6.093	1.011	

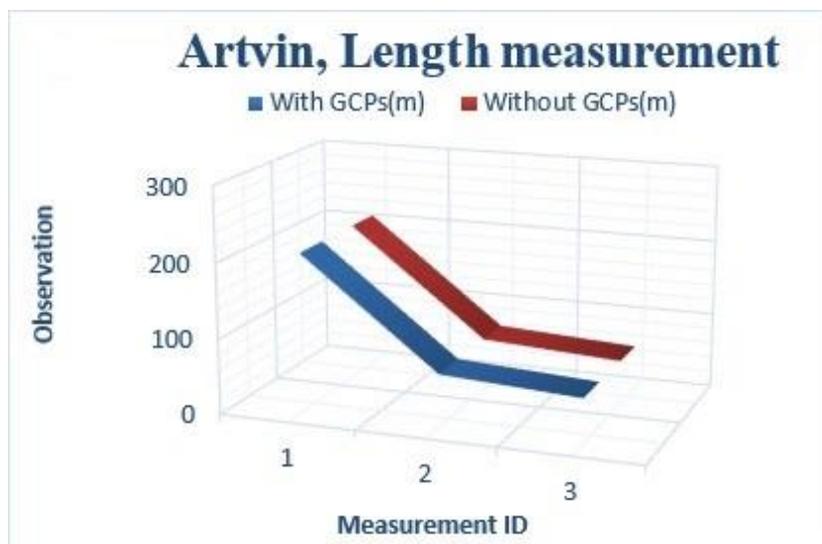**Figure 17.** Length measurements for third study area

Figure 18. Graphical vision of length measurements
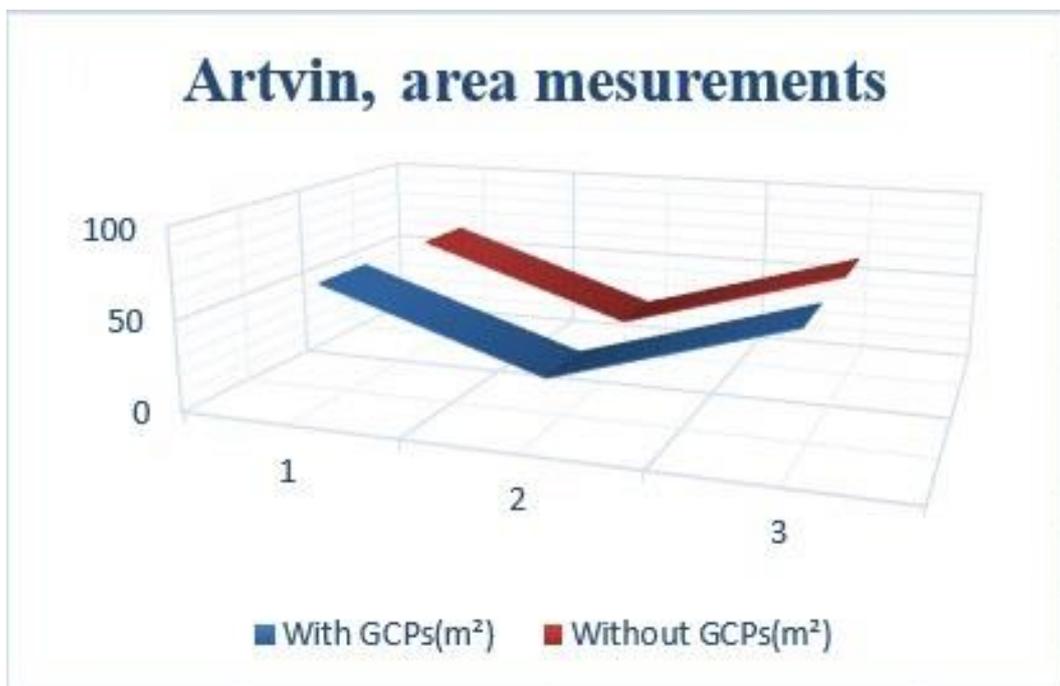
Figure 19. Areas measured in two models

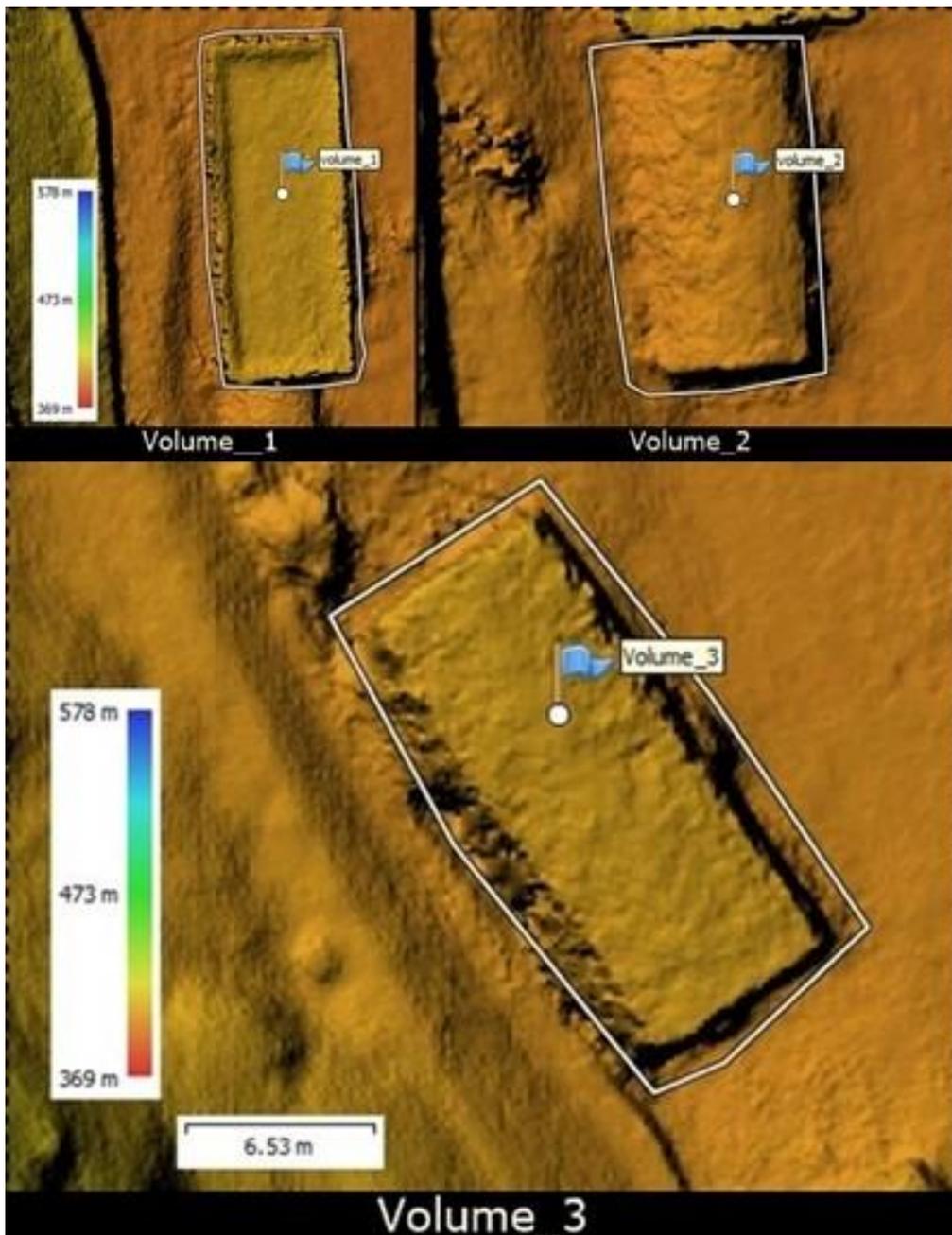**Figure 20.** Graphically representation of area measurements

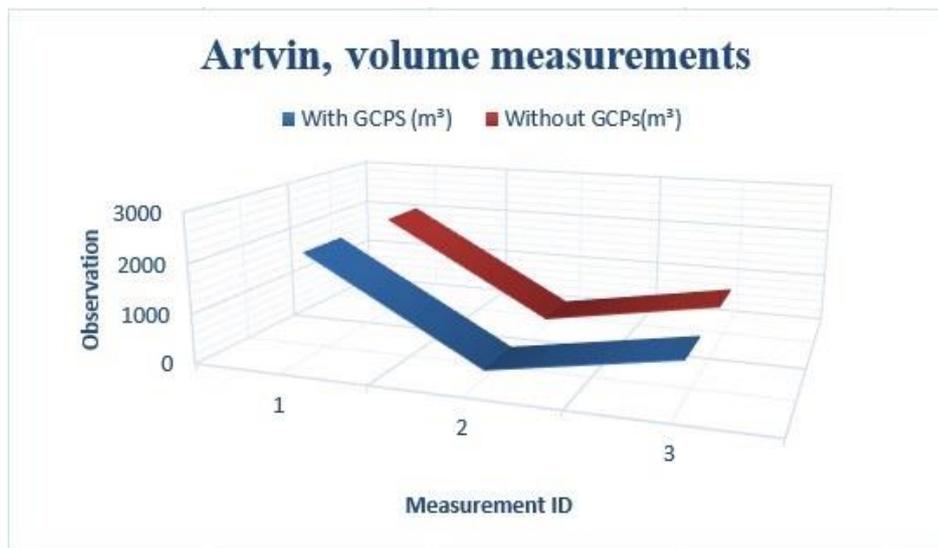**Figure 21.** Volume measurements

Figure 22. Graphic representation of volume measurements

7. Discussion

These studies were conducted to investigate the usability of 3D photogrammetric models produced without any GCPs; to reach this goal, two different areas were modelled twice each: once with GCPs and once without GCPs. To achieve the goal of this study, the lengths, areas and volumes of the same areas were measured using both models. The results obtained from the models generated with GCPs were accepted as the true values (reference values), and the results obtained from the models generated without GCPs were compared to the reference values. The relative errors as well as the RMSEs were also calculated and are given in tables above.

7.1. Length Measurement Assessment

The length measurement results provided various levels of success. The accuracy of each measurement was assessed by comparing the reference data (obtained from the model with GCPs) to the estimations determined through the photogrammetric models without GCPs. In the first study area (Sivas), length measurements were conducted on three types of terrain (flat, sloping and rocky terrain). As shown in Table 5, the length measurement errors are lower in flat areas than in inclined areas; similarly, the length measurement errors of inclined areas are lower than the errors of rocky areas. It is important to know that some objects used for the length measurements, especially those in the in inclined areas, were in close proximity to other objects and were sufficiently complex. However, overall, the first study area exhibited very promising results in measuring length, with a relative error of less than 1% and an RMSE of 0.139 m; these results are sufficiently accurate.

In the second study area (Artvin), the lengths of various objects are measured. The relative error value is 0.15%, and the RMSE is 0.153 m; these errors are also within acceptable error limits.

In an analysis of the length measurements performed using models generated with and without GCPs, no marked difference was found. The majority of relative error calculations output values less than 1%. The influence of the shape, size and configuration of the target object on the accurate estimation of the length obtained from the models without GCPs was examined in this study. Areas with greater slopes and complexity contain more errors than flat areas. In the first study area, the flat area has a majority relative error of 0.10%, whereas the inclined area has a majority relative error of 0.20%; finally, the lengths measured in the rocky area have a relative error of 0.36%. The rocky area has the highest error as well as the most complex structure in the first study area. As a result, the higher the inclination and complexity of the object area, the greater the error is.

The maximum relative errors of the length measurement between the study areas is 0.36%, which is an acceptable length accuracy. Given acceptable accuracy assessments in various fields, it is possible to conclude that photogrammetric models produced without GCPs are adequate for estimating the lengths of objects for different engineering applications, for some quantity estimations within civil engineering projects, and for disciplines that do not require very high accuracies; however, these models may not be suitable for disciplines that require very high levels of accuracy (millimetric accuracy). According to the above descriptions, we can conclude that models generated without GCPs can be used for length measurements as accurate length measurement tools.

7.2. Length Measurement Assessment

The area estimations show varying results. The accuracy of each estimation (measurement) was assessed by comparing the reference data (obtained from the model with GCPs) to the estimations determined using the photogrammetric models without GCPs.

In the area estimations, out of 8 areas measured within three study areas, five have relative errors less than 1%. One of the areas has a relative error of less than 2%, one has a relative error of 3.51%, and the last one has the maximum relative error of 5.27%. The influence of the shape and size of the area can be seen, as in the length measurements. As seen in Table 6 representing the first study area, the flat area has a majority relative error of 0.16%, whereas the inclined area has a majority relative error of 1.05%. As described for the length measurements, the higher the inclination and complexity of an object are, the greater the error is.

7.3. Volume Measurement Assessment

The results of the volume estimations obtained from the two study areas are convincing. Within the first study area (Sivas), the largest area exhibited a relative error of 0.8%, and the maximum volume estimation relative error is 6.8%. While this error appears to be slightly high, the absolute error is no more than 1.641 m^3.

The average relative error is calculated as 3.115%, and the RMSE is calculated as 2.301 m^3; these errors likely result from the failure of the software to properly model the object structure.

Similarly, for the volume estimations of the second study area, a maximum relative error of 2.01% was identified, with an RMSE of 7.061. It should be noted that the objects with the lowest-accuracy results have poor photo coverage, which is sometime caused by the location of an object in the edge of a study area or by insufficient image overlap or is sometimes due to external factors. By considering these factors, the errors can be reduced.

8. Conclusion

It is a known fact that photogrammetrically correct results can be obtained if GCPs are used. However, establishing and measuring GCPs is not always possible or preferred due to the associated costs. Today, orthophoto and digital terrain model production with unmanned aerial vehicles for use in many engineering projects can be performed without GCPs with some margin of error. The results obtained from this study and the literature review strengthen this thesis.

Based upon the obtained results, several conclusions can be made regarding the decision to accept or reject the usability of models produced without GCPs. Considering the errors calculated above, the following conclusions pertain to the ability of photogrammetric models with no GCPs.

• Photogrammetric models generated with no GCPs are usable for different engineering applications.

• Photogrammetric models produced with no GCPs can be used as accurate length-measuring tools within the modelled areas.

• Relative errors of 0.12% in the first study area (Sivas) and 0.143% in the second study area (Artvin) are obtained.

• Photogrammetric models with no GCPs can be used as accurate area-measuring tools within the modelled areas.

• The relative error in the case of the area measurement of first study area (Sivas) is 0.306%, and that of the second study area (Artvin) is 3.11%.

• Photogrammetric models with no GCPs can calculate accurate object volumes and areas with different shapes and slopes.

• A 3.115% relative error of volume measurement is calculated for the first study area (Sivas), while this value is 1.01% for the second study area (Artvin).

• The length measurements conducted by the model within flat areas are more accurate than those conducted within inclined or rocky areas.

• The area measurements conducted in flat areas are also more accurate than those conducted in inclined areas.

• The area measurements of objects with smooth shapes are more accurate than those of objects with complex shapes.

• The accuracy of the volume measurements is based on the identified base surface; if the surface is identified accurately, there is no effect on the shape or slope of the object.

• The studies above are conducted in two areas with different characteristics, such as different elevations above sea level, different climate conditions, different study area topographies, and different flight plans, but the results, accuracies, relative errors and absolute errors of these models are approximately the same. As a result, it can be indicated that the above principles (the usability of models with no GCPs) are acceptable and applicable for all conditions.

Considering the results obtained in our study, it can be seen that length, area and volume measurements can be performed with orthophotos and digital surface models produced without using GCPs with an average relative error of 0.1-3%. In light of this information, the orthophoto and digital terrain model needs of many engineering projects can be effectively met without using GCPs using images obtained by unmanned aerial vehicles.

Author contributions

Erdem Emin Maraş: Designed the study and performed the experiments, analyzed the data, wrote the manuscript. **Mohammad Noman Nasery:** Designed the study and performed the experiments.

Conflicts of interest

The authors declare no conflicts of interest.

References

1. Yastikli, N. (2007). Documentation of cultural heritage using digital photogrammetry and laser scanning. Journal of Cultural heritage, 8(4), 423-427.
2. McCarthy, J. (2014). Multi-image photogrammetry as a practical tool for cultural heritage survey and community engagement. Journal of Archaeological Science, 43, 175-185.
3. Berni, J. A., Zarco-Tejada, P. J., Suárez, L., & Fereres, E. (2009). Thermal and narrowband multispectral remote sensing for vegetation monitoring from an unmanned aerial vehicle. *IEEE Transactions on geoscience and Remote Sensing*, *47*(3), 722-738.
4. Xiang, H., & Tian, L. (2011). Development of a low-cost agricultural remote sensing system based on an autonomous unmanned aerial vehicle (UAV). *Biosystems engineering*, *108*(2), 174-190.
5. Jauregui, L. M., & Jauregui, M. (2000). Terrestrial photogrammetry applied to architectural restoration and archaeological surveys. *International Archives of Photogrammetry and Remote Sensing*, *33*(B5/1; PART 5), 401-405.
6. Bianchi, G., Bruno, N., Dall'Asta, E., Forlani, G., Re, C., Roncella, R., ... & Zerbi, A. (2016). Integrated survey for archıtectural restoratıon: A methodologıcal comparıson of two case studıes. *International Archives of the Photogrammetry, Remote Sensing & Spatial Information Sciences*, *41*, 175-182.
7. Kucukkaya, A. G. (2004). Photogrammetry and remote sensing in archeology. *Journal of Quantitative Spectroscopy and Radiative Transfer*, *88*(1-3), 83-88.
8. Guidi, G., Russo, M., Ercoli, S., Remondino, F., Rizzi, A., & Menna, F. (2009). A multi-resolution methodology for the 3D modeling of large and complex archeological areas. *International Journal of Architectural Computing*, *7*(1), 39-55.
9. Patikova, A. (2004) Digital photogrammetry in the practice of open pit mining. Int. Arch. Photogramm. Remote Sens. Spat. Inf. Sci. 34, 1-4.
10. Sheng, Y. H., Yan, Z. G., & Song, J. L. (2003). Monitoring technique for mining subsidence with digital terrestrial photogrammetry. *Journal of China University of Mining & Technology*, *32*(4), 411-415.
11. Murfitt, S. L., Allan, B. M., Bellgrove, A., Rattray, A., Young, M. A., & Ierodiaconou, D. (2017). Applications of unmanned aerial vehicles in intertidal reef monitoring. *Scientific reports*, *7*(1), 1-11.
12. Yalcin, G., & Selcuk, O. (2015). 3D city modelling with Oblique Photogrammetry Method. *Procedia Technology*, *19*, 424-431.
13. Danahy, J. (1997). A set of visualization data needs in urban environmental planning & design for

photogrammetric data. In *Automatic extraction of man-made objects from aerial and space images (II)* (pp. 357-366). Birkhäuser, Basel.

14. Döner, F. & Bıyık, C. Management of three dimensional objects in spatial database. Chamb. Surv. Cadastre Eng. Geod. Geoinf. Mag. 100, 27 (2009).

15. Yılmaz, H. M., Mutluoglu, O., Ulvi, A., Yaman, A., & Bilgilioglu, S. S. (2018). Created Tree Dimensional Model of Aksaray University Campus with Unmanned Aerial Vehicle. *Journal of Geomatics*, *3*(2), 103-107.

16. Choudhury, M. A. M., Costanzini, S., Despini, F., Rossi, P., Galli, A., Marcheggiani, E., & Teggi, S. (2019, May). Photogrammetry and Remote Sensing for the identification and characterization of trees in urban areas. In *Journal of Physics: Conference Series* (Vol. 1249, No. 1, p. 012008). IOP Publishing.

17. Wu, B., Xie, L., Hu, H., Zhu, Q., & Yau, E. (2018). Integration of aerial oblique imagery and terrestrial imagery for optimized 3D modeling in urban areas. *ISPRS journal of photogrammetry and remote sensing*, *139*, 119-132.

18. Goetz, J., & Brenning, A. (2019). Quantifying uncertainties in snow depth mapping from structure from motion photogrammetry in an alpine area. *Water Resources Research*, *55*(9), 7772-7783.

19. Chudley, T. R., Christoffersen, P., Doyle, S. H., Abellan, A., & Snooke, N. (2019). High-accuracy UAV photogrammetry of ice sheet dynamics with no ground control. *The Cryosphere*, *13*(3), 955-968.

20. Casella, V. and Franzini, M. (2016) Modelling steep surfaces by various configurations of nadir and oblique photogrammetry. ISPRS Annals of the Photogrammetry. Remote Sensing and Spatial Information Sciences, III-1, 175-182.

21. Tomaštík, J., Mokroš, M., Surový, P., Grznárová, A., & Merganič, J. (2019). UAV RTK/PPK method—An optimal solution for mapping inaccessible forested areas?. *Remote sensing*, *11*(6), 721.

22. He, F., Zhou, T., Xiong, W., Hasheminnasab, S. M., & Habib, A. (2018). Automated aerial triangulation for UAV-based mapping. *Remote Sensing*, *10*(12), 1952.

23. Gerke, M., & Przybilla, H. J. (2016). Accuracy analysis of photogrammetric UAV image blocks: Influence of onboard RTK-GNSS and cross flight patterns. *Photogrammetrie, Fernerkundung, Geoinformation (PFG)*, (1), 17-30.

24. Turk, T. & Ocalan, T. (2020). Examining the Accuracy of Photogrammetric Products Obtained by Unmanned Aerial Vehicles with PPK GNSS System with Different Approaches. Turkish Journal of Photogrammetry, 2 (1), 22-28.

25. Eling, C., Klingbeil, L., & Kuhlmann, H. (2014). Development of an RTK-GPS system for precise real-time positioning of lightweight UAVs.

26. Takasu, T. (2021) RTKLIB, Open-Source Program Package for RTK-GPS. https://github.com/tomojitakasu/RTKLIB